Int. J. Electrochem. Sci., 8 **(2013)** 5250 - 5261

International Journal of
ELECTROCHEMICAL
SCIENCE
www.electrochemsci.org

Development of a Dissolved Oxygen Sensor for Commercial Applications

Tsung-Hsuan Tsai, Cheng-Yu Yang, Shen-Ming Chen[*]

Electroanalysis and Bioelectrochemistry Lab, Department of Chemical Engineering and Biotechnology, National Taipei University of Technology, No.1, Section 3, Chung-Hsiao East Road, Taipei 106, Taiwan (ROC).
[*]E-mail: smchen78@ms15.hinet.net

Received: 1 February 2013 / *Accepted:* 7 March 2013 / *Published:* 1 April 2013

The gold nanoparticles (GNP) and functionalized carbon nanotube (*f*-CNT) film (GNP-*f*-CNT) was prepared on glassy carbon electrode (GCE) by multiple scan cyclic voltammetry. The electrochemical measurements and surface morphology of the as prepared films were studied using field emission scanning electron microscopy (FE-SEM), electrochemical impedance spectroscopy (EIS) and X-ray diffraction (XRD). The proposed film were demonstrated for the determination of dissolved oxygen using cyclic voltammetry and rotating disk electrode voltammetry. The electrocatalytic reduction of dissolved oxygen at bare GCE, *f*-CNT, GNP and GNP-*f*-CNT modified electrodes, were determined in 0.1 M pH 7 phosphate buffer solution. The dissolved oxygen electrochemical sensor exhibits a well linear response range (from 0 to 50 mg/L, R^2 = 0.9988), lowest detection limit (0.1 mg/L), high sensitivity (196.5 μA L mg^{-1} cm^{-2}) and the relative standard deviation (RSD) for determining dissolved oxygen (n = 3) was 3.8%. For the determination of dissolved oxygen, the GNP-*f*-CNT film modified GCE shows on lowest over-potential at -0.17 V. In addition, the proposed film also exhibit excellent stability and specificity.

Keywords: Gold nanoparticles, multi-walled carbon nanotube, Functionalization, Electrocatalysis, Dissolved oxygen, Modified electrodes

1. INTRODUCTION

Oxygen reduction reactions are chemically and biologically important reactions. Chemically modified electrodes have been well known for the detection of important compounds [1 – 4]. Recently, dissolved oxygen detection has potential interest in many fields. Among these we can highlight the development of new catalysis for the multi-electron reduction of oxygen with applications in biological reactions and fuel cell [5–9].

There are few traditional techniques have been proposed for the determination of dissolved oxygen, such as titration [10], colorimetry [11, 12], fluorescence [13, 14], chemiluminescence [15], and novel techniques like potentiometry [16], amperometry [17, 18], and voltammetry [19, 20]. Among these various methods, the electrochemical method gets more attention due to its good sensitivity and limited interference has got more attention [21].

The application of nanoparticles as electrocatalyst for the oxygen reduction process has been found as interesting topic. Various types of modified electrodes have been reported for the electrochemical reduction of oxygen. Such as electrocatalytic reduction and determination of dissolved oxygen at the pre-anodized screen-printed carbon electrode modified with palladium nanoparticles [22, 23], platinum nanoparticles [24], oxygen reduction at Au nanoparticles electrodeposited on different carbon substrates [25], silver/ionic liquid composite [20], gold/platinum hybrid nanoparticles supported on multi walled carbon nanotube/silica coaxial nanocables as electrocatalysts for oxygen reduction [26], gold nanoparticles dispersed into poly(aminothiophenol) as a novel electrocatalyst and CNTs [27] have been used as catalysts for the electroreduction and electrochemical detection of dissolved oxygen.

Recently, several studies have been developed aiming at the search of suitable non-platinum based electrocatalysts efficient enough to replace the costly platinum [28-29]. Among various nanoparticles, gold has been found as a promising catalyst for the oxygen reduction reaction because of its high activity for the oxygen reduction, relatively low costs and withholds the good alcohol-tolerance capacity [25, 30-32]. Numerous reports have been found for the chemical and electrochemical synthesis of gold nanomaterials which could be used as catalysts for the oxygen reduction reactions [33, 34], respectively.

Carbon nanotubes have inherently low bending stiffness and weak interaction with polymer phases and metal ions, which results in strong intermolecular interaction between individual nanotubes [35, 36]. Therefore, control over the surface polarity and the resulting interactive force between CNTs and polymer phase is necessary. In this study, a chemical surface treatment called functionalization was employed to enhance the interfacial bonding between CNTs and an epoxy matrix as well as the dispersibility of CNTs [37]. Functionalization is used to introduce reactive groups on the surface of CNTs to form covalent bonds between the reactive groups and the epoxides [38].

The aim of this work is concerned with the effect of a gold nanoparticles- functionalized MWCNT composite film (GNP-*f*-CNT) on electrode behavior. The GNP-*f*-CNT modified film has been characterized using field emission scanning electron microscopy (FE-SEM). Cyclic voltammetric (CV) and rotating disk electrode (RDE) techniques were used to study the mechanism of oxygen reduction reaction.

2. EXPERIMENTAL

2.1. Reagents

The used multi-walled carbon nanotubes (MWCNT) with an average length close to 5–20 μm and a diameter in the range of 10–15 nm and the potassium tetrachloroaurate ($KAuCl_4$, anhydrous,

97%) were purchased from Sigma–Aldrich (USA). The MWCNT were followed the functionalized process [35, 36]. All the other chemicals (Merck) used were of analytical grade (99%). Double distilled deionized water was used to prepare all the solutions. A 0.1 M phosphate buffer solution (PBS) of pH 7.0 was prepared using Na_2HPO_4 (0.1 M) and NaH_2PO_4 (0.1 M).

2.2. Apparatus

All electrochemical experiments were performed using CHI 410a potentiostats (CH Instruments, USA). The BAS GCE (η=0.3 cm in diameter, exposed geometric surface area 0.07 cm^2, Bioanalytical Systems, Inc., USA) was used. A conventional three-electrode system was used which consists of an Ag/AgCl (saturated KCl) as a reference, bare or GNT-CNT modified GCE as working and platinum wire as counter electrode. Field emission scanning electron microscope (FE-SEM) images were recorded using a HITACHI S-4700 (Japan). Electrochemical impedance studies (EIS) were performed using ZAHNER impedance analyzer (Germany). The dissolved oxygen was measured using a commercial dissolved oxygen meter 323-A (WTW Wissenschaftlich-Technische Werkstatten 2BA202, Germany). The buffer solution was entirely altered by deaerating using nitrogen gas atmosphere. The oxygen gas was purged as required and the concentrations were measured

3. RESULTS AND DISCUSSION

3.1. Electrochemical Properties of GNT-f-CNT Film and Various Scan Rate

In Fig. 1A, curve (a) indicates the CV signals of GNP-*f*-CNT/GCE, (b) GNT/GCE, (c) *f*-CNT/GCE and (a') bare GCE in 0.1 M PBS (pH 7.0). The proposed composites, (a) GNT-*f*-CNT/GCE, shows higher current and obvious peak when compared with other modified electrodes. When comparing the formal potential ($E^{0'}$), the GNT-*f*-CNT/GCE (29.5 mV) is the lowest and the redox peak is the most close. In the same buffer solution, there is no obvious response at bare GCE.

To characterize electrochemical behavior of the proposed film, GNP-*f*-CNT/GCE was examined to study how the peak current of GNP-*f*-CNT/GCE affected by different scan rate studies. As shown in Fig. 1B, the cyclic voltammograms of GNP-*f*-CNT/GCE was examined in 0.1 M PBS (pH 7) by controlling scan rates from 0.05 to 1 V/s. In the potential range from 0.4 V to -0.6 V, the GNP-*f*-CNT film exhibits a broad anodic and cathodic peak at 0.1 V and –0.3 V, respectively. It can be seen that the redox peak current increases with increase in scan rate and found linearly dependent on the scan rate from 0.05 to 1 V/s (shown in the inset (a) of Fig. 1B). The corresponding linear regression equations are: I_{pa} (μA) = 1.78v (V/s) + 84.77 (R^2=0.9997) and I_{pc} (μA) = -1.59v (V/s) – 38.91 (R^2=0.9995). As shown in inset (b) in Figure 1B, the logarithmic form of the peak current vs. scan rate (v) plot yields a gradient of I_{pa} = 0.83 and I_{pc} = 0.94, which indicates that the charge transfer was a mixed process with a near-equal contribution from the semiinfinite linear diffusion and surface process [39, 40]. It indicates that the electrochemical reaction of GNP-*f*-CNT/GCE was a surface-controlled process.

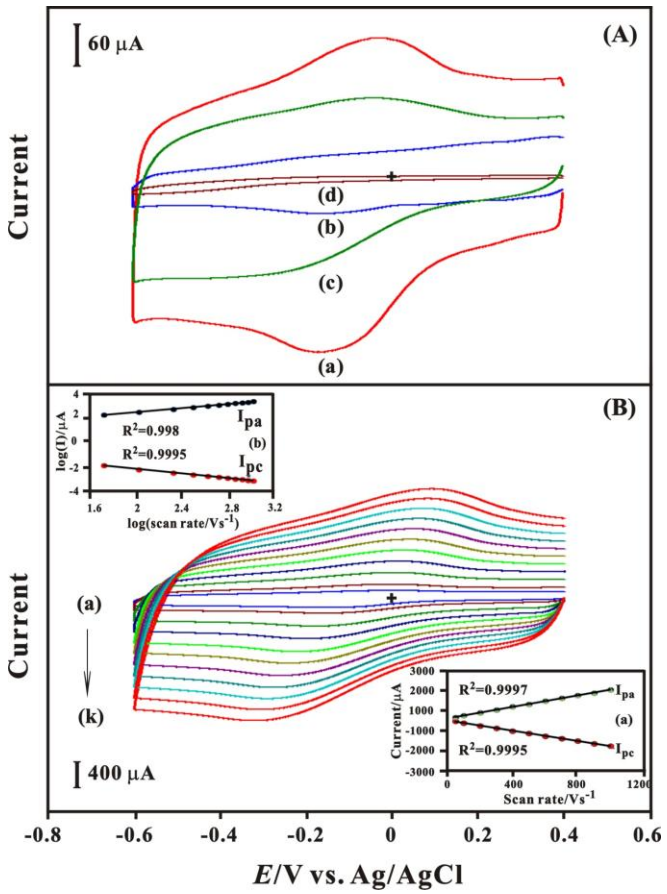

Figure 1. (A) CVs of (a) GNP-*f*-CNT/GCE, (b) GNP/GCE, (c) *f*-CNT/GCE and (a') bare GCE in 0.1 M pH 7 PBS. Potential range +0.4 to -0.6 V, Scan rate = 0.1 V/s. **(B)** Results of different scan rate studies of a GNP-*f*-CNT/GCE in 0.1 M pH 7 PBS. Scan rate in the range of a-k: 0.05-1 V/s.

3.2. FE-SEM and XRD Analysis of Various Film

The surface morphology of electrodeposited GNP-*f*-CNT has been examined using FE-SEM analysis. Here the studies could furnish the comprehensive information about the surface morphology of GNP-*f*-CNT film coated on the GCE surface. As shown in Fig. 2, the surface morphology of (A) GNP-*f*-CNT and (B) *f*-CNT films were examined by FE-SEM, respectively. As shown in Fig. 2A, the *f*-CNT film show a network structure which is distributed over the GCE during the drop casting process. The *f*-CNT film provided a substrate for successful electrodeposition of gold nanoparticles on the GCE surface (Fig. 2B). The average particle size of gold nanoparticles is in the ranges of 10–25 nm. For formation process of GNP-*f*-CNT, the functionalization of MWCNT would be slightly affected by gold-sulfur of proposed film composite in the presence of gold nanoparticles. However, it is can be seen that the gold nanoparticles is uniformly electrodeposited on the *f*-CNT film.

XRD has been employed to validate the proposed GNP-*f*-CNT structure on the ITO glass substrate. Fig. 3 shows the XRD patterns obtained for the GNP-*f*-CNT nanoparticles. There are important characteristic peaks obtained for the electrodeposited GNP-*f*-CNT film. For gold patterns, the peaks were found in 38.07°, 44.26°, 64.38° and 77.31° for Au(111), Au(200), Au(220) and

Au(311), respectively. For *f*-CNT patterns, the peaks were found at around 26.34°. All these XRD peaks clearly validate the presence of GNP-*f*-CNT on the ITO surface.

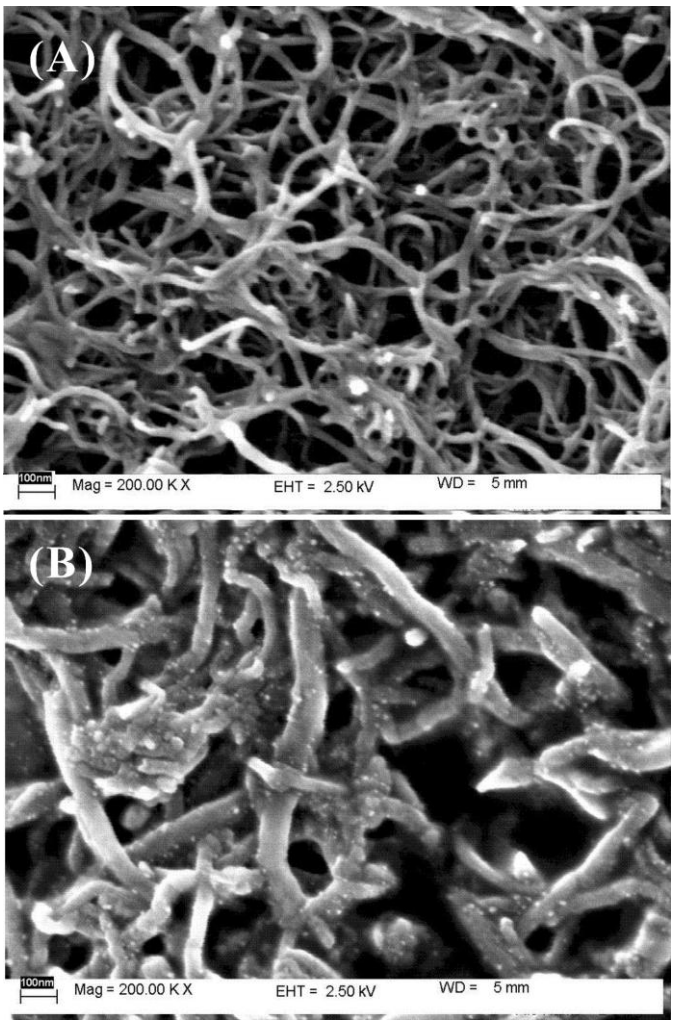

Figure 2. FE-SEM image of a **(A)** *f*-CNT film and **(B)** GNP-*f*-CNT film on GCE surface.

3.3. EIS Analysis and pH effect of Various Film

To ascertain the pH effect, the voltammetric response of GNP-*f*-CNT/GCE was studied by controlling different pH conditions (a) pH 1, (b) pH 3, (c) pH 5, (d) pH 7, (e) pH 9, (f) pH 11 and (g) pH 13. As can be seen in Fig. 4A, the formal potential ($E^{0'}$) of redox couple was found pH dependent and had a slope of −62.2 mV per pH for GNP-*f*-CNT (shown in inset of Fig. 4A) which is very close to the anticipated Nernstian value of −59 mV/pH for electrochemical processes involving the same transfer number of proton and electron [32].

The electrochemical activity of the GNP-*f*-CNT/GCE was examined using the EIS technique. Here the complex impedance can be presented as a sum of the real Z' (Ω) and imaginary Z'' (Ω) components that originate mainly from the resistance and capacitance of the cell. From the shape of an impedance spectrum, the electron transfer kinetics and diffusion characteristics can be determined. The

respective semicircle parameters correspond to the electron transfer resistance (R_{et}) and the double layer capacity (C_{dl}) nature of the modified electrode [48, 49].

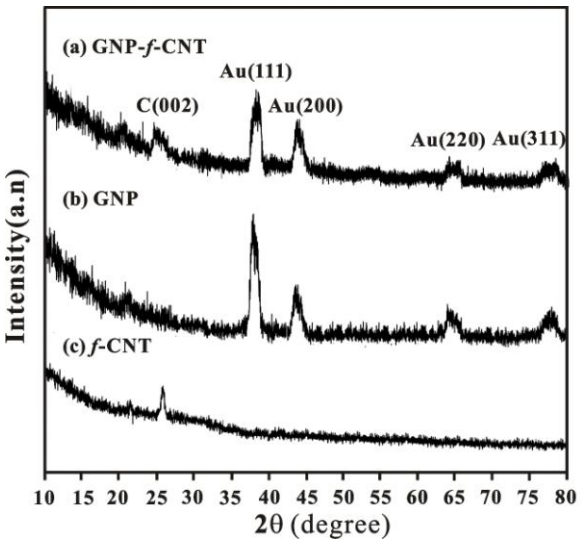

Figure 3. XRD analysis of (a) GNP-*f*-CNT film, (b) GNP film and (c) *f*-CNT film on ITO surface.

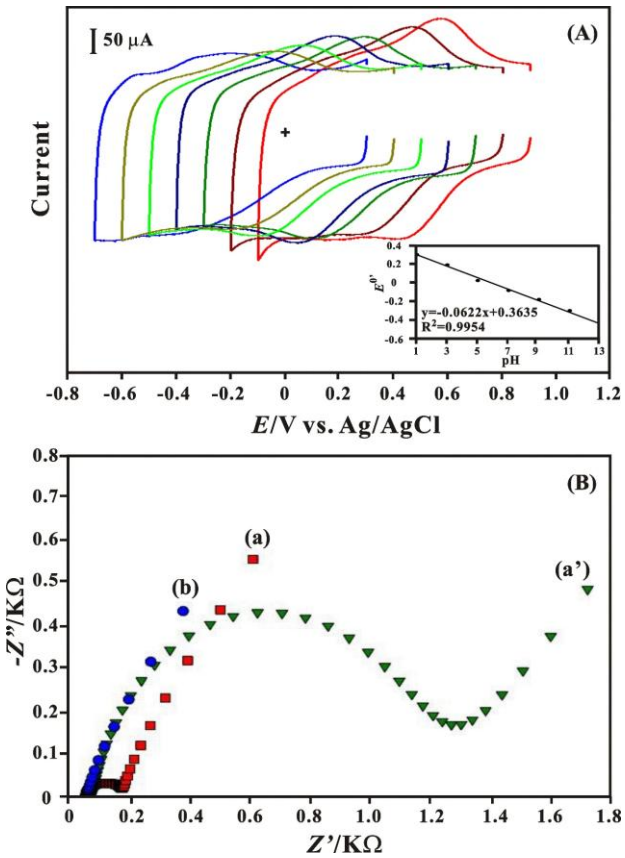

Figure 4. (A) CVs of GNP-*f*-CNT film modified GCE at a-g: pH 1, 3, 5, 7, 9, 11 and 13 solutions. Scan rate = 0.1 V/s. Inset: plot of formal potential of GNP-*f*-CNT/GCE vs. pH. **(B)** EIS curves of (a) GNP-*f*-CNT, (b) *f*-CNT film modified GCE and (a') bare GCE in 0.1 M pH 7 PBS containing 5 mM $K_3[Fe(CN)_6]/K_4[Fe(CN)_6]$.

As shown in Fig. 4B, curve (a) indicates the Nyquist plot of GNP-CNT/GCE, (b) CNT/GCE and (a') bare GCE in the presence of 5 mM $K_3[Fe(CN)_6]/K_4[Fe(CN)_6]$ in pH 7 PBS, which were performed at the open circuit potential. The *f*-CNT/GCE shows a very small depressed semicircle arc with an interfacial resistance due to the electrostatic repulsion between the charged surface and probe molecule $Fe(CN)_6^{3-/4-}$. This depressed semicircle arc (R_{et} = 132 (Z'/Ω)) clearly indicates the lower electron transfer resistance behavior compared to (a) GNP-*f*-CNT/GCE (R_{et} = 229 (Z'/Ω) and (a') bare GCE (R_{et} = 1315 (Z'/Ω)). The small depressed semicircle of *f*-CNT/GCE means that the electron transfer resistance is relative smaller than mass transfer resistance in this electrochemical system. In other words, the electron transfer is fast and mass transfer limits the system. This is because of the electron transfer resistance might be lowered by *f*-CNT. Finally, the EIS analysis clearly illustrates that the electrochemical behavior of the proposed GNP-*f*-CNT/GCE composite film is excellent.

3.4. Electrocatalytic Properties of GNP-f-CNT Film

3.4.1. Electrocatalytic Reduction of Dissolved Oxygen at GNP-f-CNT film Modified GCE

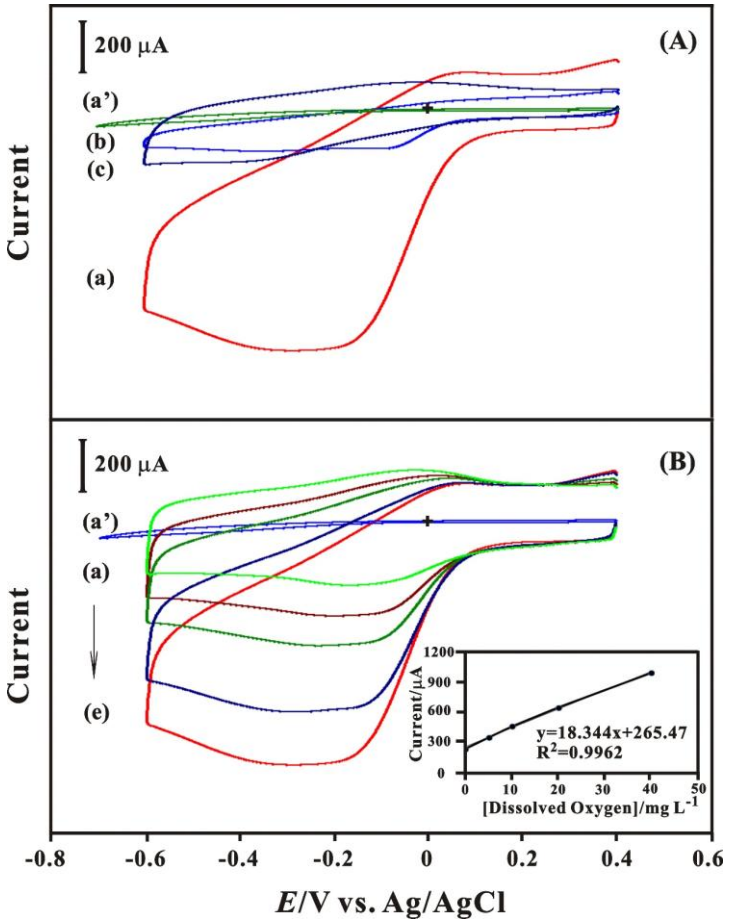

Figure 5. (A) CVs of (a) GNP-*f*-CNT/GCE, (b) GNP/GCE, (c) *f*-CNT/GCE and (a') bare GCE in 0.1 M pH 7 PBS containing 40 mg/L dissolved oxygen. **(B)** CVs of GNP-*f*-CNT modified GCE in 0.1 M pH 7 PBS containing dissolved oxygen (a) 0.0 mg/L, (b) 5 mg/L, (c) 10 mg/L, (d) 20 mg/L and (e) 40 mg/L. (a') bare GCE with 40 mg/L dissolved oxygen. Scan rate = 0.1 V/s. Inset: calibration plot of reduction current vs. concentration of dissolved oxygen.

The dissolved oxygen reduction is studied and compared with different film modified electrodes in 0.1 M PBS solution (pH 7) by cyclic voltammetry. Fig. 5A shows the cyclic voltammograms of (a) GNP-*f*-CNT/GCE, (b) GNP/GCE, (c) *f*-CNT/GCE, and (a') bare GCE examined in 0.1 M PBS (pH 7) containing 40 mg/L dissolved oxygen, respectively. The proposed composites, (a) GNP-*f*-CNT/GCE, shows high electrocatalytic reduction current for the detection of dissolved oxygen with a cathodic peak and a lower over-potential of around -0.17 V as comparing to other electrodes. By comparison, the GNT-*f*-CNT/GCE shows unique electrocatalytic ability of lower over-potential and higher electrocatalytic current better than that of GNT/GCE, *f*-CNT/GCE and bare GCE. On comparison with the (b) GNP/GCE and (c) *f*-CNT/GCE, the peak current is increased by 6.14 and 11 times. The enhanced peak current of GNP-*f*-CNT in the modified electrode is due to the presence of *f*-CNT. The *f*-CNT offers good stability, high conductivity, and acts as a good matrix. It represents the GNT-*f*-CNT film has potential to develop a dissolved oxygen sensor.

The electrocatalytic property of the GNP-f-CNT/GCE towards the reduction of dissolved oxygen was studied using CV. Fig. 5B shows the CV obtained for electrocatalytic reduction of dissolved oxygen at GNP-f-CNT/GCE in various concentrations (a) 0, (b) 5, (c) 10, (d) 20, and (e) 40 mg/L. An increase in the concentration of dissolved oxygen simultaneously produced an increase in the reduction current of dissolved oxygen in the peak of GNP-*f*-CNT/GCE. The linear depends on the I_{pc} versus concentration of dissolved oxygen is given in inset of fig. 5B. This behavior is typical of that expected for the mediated reduction. In the same solution, there was no obvious response at bare GCE electrode. All the above results indicate that GNP-*f*-CNT film modified electrode enhance the electrocatalytic reaction of dissolved oxygen.

3.4.2. Rotating Disk Technique Analysis of Dissolved Oxygen Electrocatalysis by GNP-f-CNT Film

The RDE technique was employed for the detection of dissolved oxygen in 0.1 M pH 7 PBS [50, 51]. The rotation speed of GNP-*f*-CNT film modified GCE was set to be as 1000 rpm and the reduction progress has been examined within the potential of +1.0 to -0.6 V, scan rate = 0.1 V/s. Curve a–k of Fig. 6A show that there is a linearly increase in the cathodic peak current at GNP-*f*-CNT/GCE for the increasing concentrations of dissolved oxygen (0 to 50 mg/L) in 0.1 M pH 7 PBS. The reduction peak current vs. concentration of the dissolved oxygen has been plotted and shown in the Inset of Fig. 6A. The calibration plot is linear in the entire range (0 to 50 mg/L, R^2=0.9988) of dissolved oxygen concentration with a sensitivity of 196.5 μA L mg^{-1} cm^{-2}. The detection limit was found to be 0.1 mg/L and the relative standard deviation (RSD) for determining dissolved oxygen (n = 3) was 3.8%, respectively. These results shows that the electro-catalytic oxygen reduction occured at GNP-*f*-CNT film modified GCE. As a next step, GNP-*f*-CNT film modified GCE was used to determination the dissolved oxygen of commercial drinking water products (sample A-E) with 0.1 M Na_2HPO_4, NaH_2PO_4 as electrolyte. As compared the concentration of dissolved oxygen, a commercially available dissolved oxygen meter (WTW, 323-A) was used for the reference standard. As shown in table 1, the average recoveries of sample A-E were from 92.7% to 102.4%. This results

shows that the GNP-*f*-CNT film modified GCE was successfully employed for the dissolved oxygen sensor in the commercially available drinking water products.

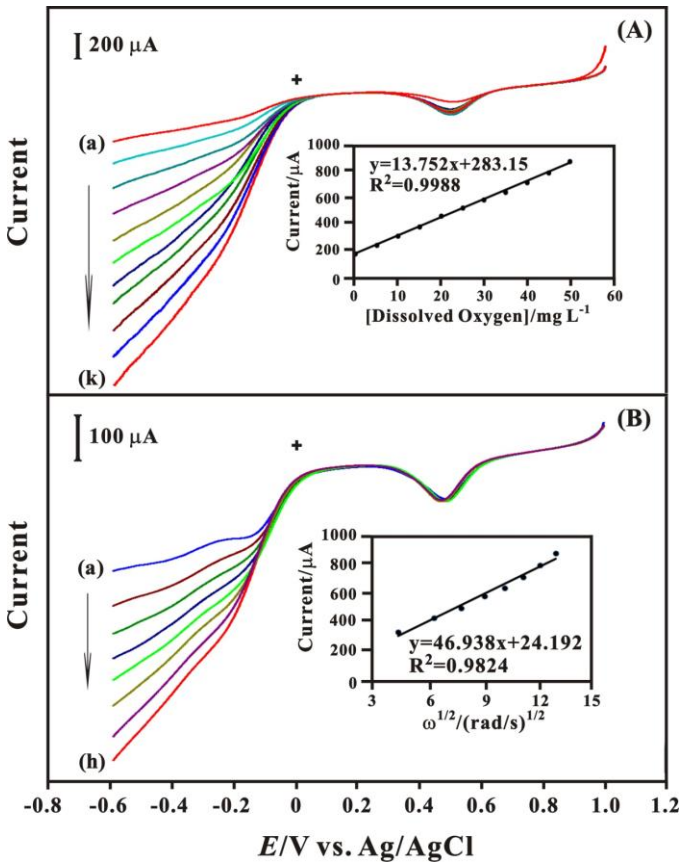

Figure 6. (A) RDE voltammograms of GNP-*f*-CNT film for the determination of dissolved oxygen in 0.1 M pH 7 PBS. Dissolved oxygen concentrations were in the range of (a–k): 0, 5, 10, 15, 20, 25, 30, 35, 40, 45 and 50 mg/L. Rotating speed: 1000 rpm. Inset: calibration plot of reduction current vs. concentration of dissolved oxygen. **(B)** RDE voltammograms of GNP-*f*-CNT film in 0.1 M pH 7 PBS containing 50 mg/L dissolved oxygen at different electrode rotation rate speed: (a) 200, (b) 400, (c) 600, (d) 800, (e) 1000, (f) 1200 (g) 1400 and (h) 1600 rpm.

Table 1. Recoveries for the determination of dissolved oxygen in various commercial drinking water products (n = 3).

Sample NO.	GNP-CNT Film (mg/L)	WTW 323-A Meter (mg/L)	Average Recovery (%)	RSD (%)
A	36.2	37.9	95.5	7.6
B	37.8	38.6	97.9	4.3
C	21.1	20.6	102.4	5.1
D	17.9	19.3	92.7	7.1
E	13.6	14.5	93.8	6.8

Fig. 6B shows RDE voltammograms of 178.4 μM dissolved oxygen on GNP-*f*-CNT film modified electrode at different rotation rates. The catalytic current of oxygen reduction increases with

increasing electrode rotation speed ((a) 200, (b) 400, (c) 600, (d) 800, (e) 1000, (f) 1200, (g) 1400 and (h) 1600 rpm) as shown in Levich plot (inset of Fig. 6B) indicates that the oxygen reduction reaction was diffusion controlled process on the modified electrode. The I_{pa} was found increased linearly with the rotation rate with slope 46.94 μA (rad s^{-1})$^{-1/2}$ and the diffusion coefficient for oxygen calculated from the Levich plot was found to be 1.92 x 10^{-6} cm^2 s^{-1}.

Table 2. Comparison of sensing abilities for dissolved oxygen with different modified electrodes.

Modified Electrode	E_{pc} (mV)	LCR (**mg/L**)	LOD (**mg/L**)	Sensitivity (μA L mg^{-1} cm^{-2})	Ref.
MWCNTs-NF-Hb/GCE	-200 (Ag/AgCl)	0.8-8	---	513	[41]
nano-Ag/BMT-Nf/GCE	-440 (Ag/AgCl)	0.3-3.4	0.2	535	[20]
CNF/GCE	-308 (Ag/AgCl)	0.003-0.249	0.002	22.6	[42]
Nickel-salen polymer/PtE	-250 (SCE)	3.95-9.2	0.71	14.6	[43]
SiO2/SnO2/MnPc	-300 (SCE)	0.2-8.1	---	212.5	[44]
CoTSPc/PLL/GCE	-300 (SCE)	0.2-8.0	0.07	18.3	[45]
Vitamin B12/GCE	-400 (Ag/AgCl)	0.48-16	0.29	7.04	[46]
SiSb/CoTmPyP/CPE	-250 (SCE)	1-12.8	---	0.096	[47]
GNP-*f*-CNT/GCE	-170 (Ag/AgCl)	0-50	0.1	196.5	This work

Table 2 shows the comparison of the determination of dissolved oxygen by various electrochemical modified electrodes [20, 41-47]. Compared with other modified electrodes in buffer solution, GNP-*f*-CNT film modified GCE has the lowest over-potential and high sensitivity for the determination of dissolved oxygen. Similarly, GNP-*f*-CNT film modified GCE for the detection of dissolved oxygen also has high linear concentration range (LCR) in 0.1 M pH 7 PBS.

4. CONCLUSION

A stable and simple film of GNP was successfully electrodeposited on *f*-CNT modified GCE surface by continuous cycling in 0.1 M H_2SO_4 solution containing $KAuCl_4$. The surface analysis of the proposed film by FE-SEM shows that the GNP-*f*-CNT film was uniform. The composite film can be used for the electrocatalytic reduction of dissolved oxygen and investigated using the RDE methods. The GNP-*f*-CNT film facilitated the reduction of dissolved oxygen with a low over-potential of –0.17 V and a sensitivity of 196.5 μA L mg^{-1} cm^{-2}. The GNP-*f*-CNT film modified GCE also successfully employed for the dissolved oxygen sensor in the commercial drinking water products. In addition, the copper GNP-*f*-CNT/GCE exhibit a distinct advantage of simple preparation, specificity, stability and reproducibility.

ACKNOWLEDGEMENTS
We acknowledge NSC (project no. NSC982113M027006MY3) and OXY YOUNG Co., Ltd. provide the commercial drinking water products, Taiwan (ROC).

References

1. R.W. Murray, *Ann. Rev. Mater. Sci.*, 14 (1984) 145.
2. R.W. Murray, A.G. Ewing and R.A. Durst, *Anal. Chem.*, 59 (1987) 379A.
3. P. Shakkthivel and S.M. Chen, *Biosens. Bioelectron.*, 22 (2007) 1680.
4. S. Thiagarajan, T.H. Tsai and S.M. Chen, *Biosens. Bioelectron.*, 24 (2009) 2712.
5. G.F. Zuo, H.Q. Yuan, H.D. Yang, R.X. Zuo and X.Q. Lu, *J. Mol. Catal. A: Chem.*, 269 (2007) 46.
6. K.M. Kadish, J.G. Shao, Z.P. Ou, L. Fremond, R.Q. Zhan, F. Burdet, J.M. Barbe, C.P. Gros and R. Guilard, *Inorg. Chem.*, 44 (2005) 6744.
7. C.S. Martin, T.R.L. Dadamos and M.F.S. Teixeira, *Sens. Actuators B: Chem.*, 175 (2012) 111.
8. T.H. Tsai, S.H. Wang and S.M. Chen, *J. Electroanal. Chem.*, 659 (2011) 69.
9. T.H. Tsai, S.H. Wang and S.M. Chen, *Int. J. Electrochem. Sci.*, 6 (2011) 1655.
10. C. Oudot, R. Gerard, P. Morin and I. Gningue, *Limnol. Oceanogr.*, 33 (1988) 146.
11. S.C. Pai, G.C. Gong and K.K. Liu, *Mar. Chem.*, 41 (1993) 343.
12. Y. Suzuki, H. Nishide and E. Tsuchida, *Macromolecules*, 33 (2000) 2530.
13. A.K. McEvoy, C.M. McDonagh and B.D. MacCraith, Analyst, 121 (1996) 785.
14. R.T. Bailey, F.R. Cruickshank, G. Deans, R.N. Gillanders and M.C. Tedford, *Anal. Chim. Acta*, 487 (2003) 101.
15. X.D. Shao, H.Y. Liu, X.F. Gao, W.Q. Chen and Z.H. Song, *Chemical Papers.*, 61 (2007) 353.
16. W. Granéli and E. Granéli, *Marine Biology*, 108 (1991) 341.
17. K.C. Gulla, M.D. Gouda, M.S. Thakur and N.G. Karanth, *Biochim. Biophys. Acta*, 1597 (2002) 133.
18. F.S. Damos, R.C.S. Luz, A.A. Tanaka and L.T. Kubota, *Anal. Chim. Acta*, 664 (2010) 144.
19. R. Reinke and J. Simon, *Aanl. Bioanal. Chem.*, 374 (2002) 1256.
20. T.H. Tsai, S. Thiagarajan and S.M. Chen, *Electroanalysis*, 22 (2010) 680.
21. M.S. Lin, H.J. Leu and C.H. Lai, *Anal. Chim. Acta*, 561 (2006) 164.
22. Y.H. Lin, X.L. Cui and X.R. Ye, *Electrochem. Commun.*, 7 (2005) 267.
23. C.C. Yang, A. Senthil Kumar and J.M. Zen, *Electroanalysis*, 18 (2006) 64.
24. H.F. Cui, J.S. Ye, W.D. Zhang, J. Wang and F.S. Sheu, *J. Electroanal. Chem.*, 577 (2005) 295.
25. M.S. El-Deab, T. Sotomura and T. Ohsaka, *Electrochim. Acta*, 52 (2006) 1792.
26. S. Guo, S. Dong and E. Wang, *J. Phys. Chem. C.*, 112 (2008) 2389.
27. J.S. Ye, Y. Wen, W.D. Zhang, H.F. Cui, L.M. Gan, G.Q. Xu and F.S. Sheu, *J. Electroanal. Chem.*, 562 (2004) 241.
28. L. Mao, K. Arihara, T. Sotomura and T. Ohsaka, *Electrochim. Acta*, 49 (2004) 2515.
29. F.P. Hu, X.G. Zhang, F. Xiao and J.L. Zhang, Carbon, 43 (2005) 2931.
30. T.H. Tsai, S. Thiagarajan and S.M. Chen, *J. Appl. Electrochem.*, 40 (2010) 493.
31. T.H. Tsai, S. Thiagarajan and S.M. Chen, *J. Appl. Electrochem.*, 40 (2010) 2071.
32. T.H. Tsai, K.C. Lin and S.M. Chen, *Int. J. Electrochem. Sci.*, 6 (2011) 2672.
33. O. Tripachev, V. Bogdanovskaya, M. Tarasevich and V. Andoralov, *J. Electroanal. Chem.*, 683 (2012) 21.
34. M.I. Awad and T. Ohsaka, *J. Power Sources.*, 226 (2013) 306.
35. K.C. Lin, T.H. Tsai and S.M. Chen, *Biosens. Bioelectron.*, 26 (2010) 608.
36. C.Y. Yang, S.M. Chen, T.H. Tsai and B. Unnikrishnan, *Int. J. Electrochem. Sci.*, 7 (2012) 12796.
37. S. Thiagarajan, T.H. Tsai and S.M. Chen, *Biosens. Bioelectron.*, 24 (2009) 2712.
38. Z. Yaping, Z. Aibo, C. Qinghua, Z. Jiaoxia and N. Rongchang, *Mater. Sci. Eng. A.*, 435 (2006)

145.
39. R.W. Murray, *in Electroanalytical Chemistry*, Marcel Dekker, New York (1984) Vol. 13 (Ed: A. J. Bard), pp. 191-386.
40. T.H. Tsai, T.W. Chen and S.M. Chen, *Electroanalysis*, 22 (2010) 1655.
41. Y. Liu, T. Han, C. Chen, N. Bao, C.M. Yu and H.Y. Gu, *Electrochim. Acta*, 56 (2011) 3238.
42. L. Wu, X. Zhang and H. Ju, *Biosens. Bioelectron.*, 23 (2007) 479.
43. C.S. Martin, T.R.L. Dadamos and M.F.S. Teixeira, *Sens. Actuators B: Chem.*, 175 (2012) 111.
44. L.S.S. Santos, R. Landers and Y. Gushikem, *Talanta*, 85 (2011) 1213.
45. R. de C.S. Luz, F.S. Damos, A.A. Tanaka and L.T. Kubota, *Sens. Actuators B: Chem.*, 114 (2006) 1019.
46. M.S. Lin, H.J. Leu and C.H. Lai, *Anal. Chim. Acta*, 561 (2006) 164.
47. E.S. Ribeiro, S.L.P. Dias, Y. Gushikem and L.T. Kubota, *Electrochim. Acta*, 49 (2004) 829.
48. H. Zhang, X. Wang, R. Jia, J. Hou, W. Guo, *Int. J. Electrochem. Sci.*, 8 (2013) 1262.
49. J. Ma, X. Wang, X. Jiao, *Int. J. Electrochem. Sci.*, 7 (2012) 1556.
50. I. Kruusenberg, L. Matisen and K. Tammeveski, *Int. J. Electrochem. Sci.*, 8 (2013) 1057.
51. A. Ezeta-Mejía, J.M. Mora-Hernández, J.M. Hallen-López and E.M. Arce-Estrada, *Int. J. Electrochem. Sci.*, 8 (2013) 2044.